

## Article

# Colloidal Synthesis and Optical Properties of Cs<sub>2</sub>CuCl<sub>4</sub> Nanocrystals

Wanying Gu <sup>1,†</sup>, Yicheng Zeng <sup>1,†</sup>, Yuan Deng <sup>1</sup>, Pan Huang <sup>1</sup>, Geyu Jin <sup>1</sup>, Fangze Liu <sup>2</sup>, Jing Wei <sup>1</sup>   
and Hongbo Li <sup>1,\*</sup>

<sup>1</sup> School of Materials Science and Engineering, Beijing Institute of Technology, Beijing 100081, China

<sup>2</sup> Advanced Research Institute of Multidisciplinary Sciences, Beijing Institute of Technology, Beijing 100081, China

\* Correspondence: hongbo.li@bit.edu.cn

† These authors contributed equally to this work.

**Abstract:** Lead-free copper halide perovskite nanocrystals (NCs) are emerging materials with excellent photoelectric properties. Herein, we present a colloidal synthesis route for orthorhombic Cs<sub>2</sub>CuCl<sub>4</sub> NCs with a well-defined cubic shape and an average diameter of 24 ± 2.1 nm. The Cs<sub>2</sub>CuCl<sub>4</sub> NCs exhibited bright, deep blue photoluminescence, which was attributed to the Cu(II) defects. In addition, passivating the Cs<sub>2</sub>CuCl<sub>4</sub> NCs by Ag<sup>+</sup> could effectively improve the photoluminescence quantum yield (PLQY) and environmental stability.

**Keywords:** Cs<sub>2</sub>CuCl<sub>4</sub> nanocrystals; Ag passivation; photoluminescence quantum yield; stability

## 1. Introduction

Lead halide perovskite nanocrystals (NCs) with a general formula of APbX<sub>3</sub> (A = Cs, methylammonium or formamidinium, X = Cl, Br or I) have attracted a lot of attention for a variety of optoelectric applications such as solar cells [1], light-emitting diodes (LEDs) [2], lasers [3], photocatalysis [4,5] and photodetectors [6]. They have many advantages, including low-temperature solution processability, tunable direct bandgap, high optical absorption coefficients, high defect tolerance, long carrier lifetimes and diffusion length [7–10]. Their properties can be conveniently tuned by changing the A site anions or X site cations. Lead perovskites, especially perovskite LEDs (PeLEDs), are widely studied due to their advantages of high color purity, wide color gamut, high efficiency and low cost [11–15]. At present, the external quantum efficiencies (EQEs) of red and green PeLEDs have exceeded 20%, reaching the industrial standard. However, the EQEs of blue PeLEDs are lower than red and green PeLEDs [16–22], which is mainly due to the deep level defects originating from the large band-gap of blue-emitting perovskite NCs, and the highest EQE (12.3%) of blue PeLEDs was achieved by growing a bipolar shell to strongly confine CsPbBr<sub>3</sub> NCs and reduce the trap density [22].

Despite the rapid development of blue PeLEDs, their further applications are hindered by the inherent toxicity of the metal element lead [23]. Therefore, a lot of effort has been devoted to reducing or substituting lead with less- or nontoxic metals. For example, using Sn<sup>2+</sup> or Ge<sup>2+</sup> to substitute Pb<sup>2+</sup> and form CsSnX<sub>3</sub> or CsGeX<sub>3</sub> NCs has been widely studied [24,25]. However, the stability of this technique is relatively low due to the Sn<sup>2+</sup> or Ge<sup>2+</sup> being easily oxidized into Sn<sup>4+</sup> or Ge<sup>4+</sup> in air and generating defects in Sn/Ge based perovskites [26–28]. Using isoelectronic Bi<sup>3+</sup> or Sb<sup>3+</sup> to replace Pb<sup>2+</sup> is another approach. For example, Sb<sup>3+</sup> and Bi<sup>3+</sup> ions can form Cs<sub>3</sub>M(III)<sub>2</sub>X<sub>9</sub> (M = Sb or Bi) structures [29–31]. These perovskites generally exhibit deep blue emission and high air stability, and Ag<sup>+</sup> has been shown to be able to improve the PLQY of Cs<sub>3</sub>Bi<sub>2</sub>Br<sub>9</sub> NCs through reducing the surface trap density [30]. In addition, combining a univalent ion with a trivalent to replace two Pb ions can form double perovskites Cs<sub>2</sub>M(I)M(III)X<sub>6</sub> (M<sup>+</sup> = Ag<sup>+</sup>, Na<sup>+</sup>; M<sup>3+</sup> = In<sup>3+</sup>, Bi<sup>3+</sup>; X = Cl, Br, I), which are promising alternative lead-free materials. However, due



**Citation:** Gu, W.; Zeng, Y.; Deng, Y.; Huang, P.; Jin, G.; Liu, F.; Wei, J.; Li, H. Colloidal Synthesis and Optical Properties of Cs<sub>2</sub>CuCl<sub>4</sub> Nanocrystals. *Crystals* **2023**, *13*, 864. <https://doi.org/10.3390/cryst13060864>

Academic Editor: Alessandro Chiasera

Received: 5 May 2023

Revised: 18 May 2023

Accepted: 22 May 2023

Published: 24 May 2023



**Copyright:** © 2023 by the authors. Licensee MDPI, Basel, Switzerland. This article is an open access article distributed under the terms and conditions of the Creative Commons Attribution (CC BY) license (<https://creativecommons.org/licenses/by/4.0/>).

to their inherent indirect band gap property, their PLQYs are lower than lead halide perovskites [32–35]. Compared with  $\text{Cs}_2\text{M}(\text{I})\text{M}(\text{III})\text{X}_6$  perovskites, the vacancy-ordered layered double perovskites with a formula of  $\text{Cs}_4\text{M}(\text{II})\text{M}(\text{III})_2\text{X}_{12}$  ( $\text{M}(\text{II}) = \text{Cu}^{2+}, \text{Mn}^{2+}$ , etc.) have the advantages of a highly tunable composition, direct band gap and outstanding structural stability [36–39]. They consist of a layer of  $[\text{M}(\text{II})\text{X}_6]^{4-}$  octahedrons sandwiched between two layers of  $[\text{M}(\text{III})\text{X}_6]^{3-}$  octahedrons.  $\text{Cs}_4\text{CuSb}_2\text{Cl}_{12}$  NCs with a direct band gap of 1.79 eV has been successfully synthesized using the hot injection method [36]. The  $\text{Cs}_4\text{CuSb}_2\text{Cl}_{12}$  NCs can be used as high-speed photodetectors with ultra-fast photo response and narrow bandwidth due to their superior charge transport characteristics and solution processability [36]. Similarly,  $\text{Cs}_4\text{CuIn}_2\text{Cl}_{12}$  NCs were synthesized with the water-assisted hot injection method [37]. However, they generally exhibited low PLQY due to the strong self-trapping exciton effect originating from their layered structure [39].

Cu-based perovskite NCs are another important group of materials for replacing lead perovskites due to their abundant resources and low toxicity. Due to the relatively small ionic radius of Cu, substituting Pb with Cu tends to form zero-dimensional structures [40]. Ternary Cu halide perovskites are another group of environmentally friendly materials due to their low cost, high PL intensity and adjustable emission wavelength [41–46]. Because of the two valence states and low coordination number of Cu ions, the ternary Cu halide perovskites can form different crystal structures, including  $\text{Cs}_3\text{Cu}_2\text{X}_5$  ( $\text{X} = \text{Cl}, \text{Br}, \text{I}$ ),  $\text{CsCu}_2\text{I}_3$ ,  $\text{A}_2\text{CuX}_3$  ( $\text{A} = \text{K}, \text{Rb}$ ;  $\text{X} = \text{Cl}, \text{Br}, \text{I}$ ) and  $\text{Cs}_2\text{CuX}_4$ .  $\text{Cs}_3\text{Cu}_2\text{X}_5$  ( $\text{X} = \text{Cl}, \text{Br}, \text{I}$ ) NCs and  $\text{CsCu}_2\text{I}_3$ , for example, have been widely studied for their excellent optical properties. In 2019, Han et al. synthesized  $\text{CsCu}_2\text{I}_3$  nanorods (NRs) and  $\text{Cs}_3\text{Cu}_2\text{I}_5$  NCs using the hot injection method at different reaction temperatures [41]. The  $\text{Cs}_3\text{Cu}_2\text{I}_5$  NCs synthesized at 70 °C exhibit bright blue emissions at 441 nm with a PLQY of 67%, while the  $\text{CsCu}_2\text{I}_3$  NRs exhibit yellow emissions at 553 nm with a PLQY of 5%. Deep blue PeLEDs based on  $\text{Cs}_3\text{Cu}_2\text{I}_5$  NCs have shown a high EQE of 1.12% [42]. In contrast to lead halide perovskites, replacing I with Br and Cl tends to redshift the emission wavelength of  $\text{Cs}_3\text{Cu}_2\text{X}_5$  NCs, and  $\text{Cs}_3\text{Cu}_2\text{Br}_5$  and  $\text{Cs}_3\text{Cu}_2\text{Cl}_5$  NCs exhibit bright blue and green emissions at 458 nm and 521 nm, respectively [43]. However, their poor air stability significantly limits their further applications [43]. Li et al. [44] studied the effects of reaction temperature and ligand concentration on the structure of ternary Cu halide perovskites. Since the complexes formed by  $\text{Cu}^+$  and OA or OLA can exhibit linear, triangular or tetrahedral shapes with different barrier potentials, the crystal structure of NCs is determined by the combined effect of reaction temperature and ligand concentration. High reaction temperatures and low ligand concentration are conducive to the formation of  $\text{Cs}_3\text{Cu}_2\text{I}_3$ , while low reaction temperatures and high ligand concentration are conducive to the formation of  $\text{Cs}_3\text{Cu}_2\text{I}_5$ . In 2021, White et al. [45] reported the synthesis of  $\text{Rb}_2\text{CuX}_3$  ( $\text{X} = \text{Cl}, \text{Br}$ ) colloidal NCs with PL peaks around 400 nm using ligand assisted reprecipitation at room temperature. Ealpert et al. [46] also synthesized  $\text{K}_2\text{CuX}_3$  NCs with near UV to deep blue emission with the ligand-assisted reprecipitation method, and the PLQY of  $\text{K}_2\text{CuCl}_3$  also reached near 100%.

$\text{Cs}_2\text{CuCl}_4$  is a recently studied material with excellent blue emission properties [47–50]. The synthesis of  $\text{Cs}_2\text{CuX}_4$  ( $\text{X} = \text{Cl}, \text{Br}$ , and  $\text{Br}/\text{I}$ ) spherical quantum dots with blue-green emission was first reported by Yang et al. [48] using an improved ligand-assisted reprecipitation technique at room temperature. By changing the halide composition and precursor ratios, the emission peak can be tuned from 385 nm to 504 nm. In order to solve the low solubility of CsBr and CsCl in polar solvents, Kar et al. [49] used water as a solvent to synthesize square-shaped  $\text{Cs}_2\text{CuCl}_4$  nanoplates with deep blue PL at 434 nm. Compared with the ligand-assisted reprecipitation technique, the hot injection method could better control the reaction process and achieve NCs with a more uniform crystal size and high crystal quality [8]. Using the hot injection method, Booker et al. [50] synthesized mixed phases of  $\text{CsCuCl}_3$  and  $\text{Cs}_2\text{CuCl}_4$  NCs with bright green emissions. At present, the synthesis of uniform and pure  $\text{Cs}_2\text{CuCl}_4$  NCs with the hot injection method has not been reported.

Herein, we developed the synthesis of pure phase  $\text{Cs}_2\text{CuCl}_4$  NCs and examined its optical properties. The colloidal  $\text{Cs}_2\text{CuCl}_4$  NCs had a uniform size and excellent optical properties. We found that  $\text{Cs}_2\text{CuCl}_4$  NCs have a wide band gap of 4.36 eV and show a bright, deep blue PL at 434 nm with a PLQY of 28.8% at room temperature. In addition, we show here that the PLQY of  $\text{Cs}_2\text{CuCl}_4$  NCs can be greatly improved to 42% with  $\text{Ag}^+$  passivation. The air stability of  $\text{Ag}^+$ -treated  $\text{Cs}_2\text{CuCl}_4$  NCs were also greatly improved. After 15 days' storage in air (average temperature 25 °C, humidity 50%), 75% of their initial PLQY was retained.

## 2. Materials and Methods

### 2.1. Materials

Cesium acetate ( $\text{Cs}(\text{OAc})$ , 99.9%), copper(II) acetate ( $\text{Cu}(\text{ac})_2$ , 99.9%), silver acetate ( $\text{Ag}(\text{ac})$ , 99.99%), benzoyl chloride (Bz-Cl, 98%) and benzoyl bromine (Bz-Br, 99%) were purchased from Aladdin (Shanghai, China). The 1-octadecene (ODE, 90%), oleylamine (OLA, 70%) and oleic acid (OA, 90%) were purchased from Aldrich (Taufkirchen, Germany). All the chemicals and solvents were used without further purification.

### 2.2. Preparation of Ag-OLA Solution

$\text{Ag}(\text{ac})$  (25 mg) was loaded into a 50 mL three-neck flask along with ODE (10 mL) and OLA (1 mL). The mixture was degassed for 0.5 h at 30 °C until the  $\text{Ag}(\text{ac})$  dissolved completely.

### 2.3. Synthesis of $\text{Cs}_2\text{CuCl}_4$ NCs

In a typical synthesis,  $\text{Cs}(\text{OAc})$  (13.4 mg),  $\text{Cu}(\text{ac})_2$  (18.2 mg), OA (1 mL), OLA (0.5 mL) and ODE (5 mL) were mixed in a 50 mL flask and dried for 30 min under vacuum at 100 °C. Then, the reaction flask was heated to 120 °C in  $\text{N}_2$  atmosphere, when 48  $\mu\text{L}$  Bz-Cl dispersed in 0.5 mL of degassed ODE were injected inside the flask. After 10 s, the solution was cooled down using an ice-water bath. The resulting mixtures of  $\text{Cs}_2\text{CuCl}_4$  NCs were centrifuged for 5 min at  $8000\times g$  rpm. The precipitate was redissolved in hexane and centrifuged at  $8000\times g$  rpm for 5 min to remove undissolved species. The final supernatant was collected for further analysis.

### 2.4. Synthesis of the Ag Passivation Reagent

For UV-Vis and PL spectra of NCs before and after Ag passivation, the as-prepared  $\text{Cs}_2\text{CuCl}_4$  NCs (200  $\mu\text{L}$ ) were mixed with hexane (3 mL) in the cuvette, and then different amounts of Ag-OLA solution were injected and stirred for 2 min.

### 2.5. Characterizations

UV-Vis absorption spectra were characterized with a UV 2310-II spectrophotometer (Tianmei, Shanghai, China). The PL spectra were collected with a F-380 spectro-fluorometer (Gangdong, Tianjin, China). Absolute PLQY values were checked with an FS5 Spectrofluorometer equipped with an integrating sphere (Edinburgh Instruments, Livingston, England). Transmission electron microscopy (TEM) images were acquired with a JEM-2100 with an accelerating voltage of 200 kV (JEOL, Tokyo, Japan). X-ray diffraction (XRD) characterization was achieved with a D8 Focus X-ray diffractometer (Bruker, Billerica, MA, USA). X-ray photo-electron spectroscopy (XPS) was conducted on a QUANTERA-II SXM spectrometer (ULVAC-PHI, Maozaki, Japan). Fourier transform infrared spectroscopy (FTIR) was conducted on a TG209F1 spectrophotometer (Netzsch, Selb, Germany).

## 3. Results and Discussion

In this approach,  $\text{Cs}_2\text{CuCl}_4$  NCs were synthesized using a modified hot-injection method. The optical properties of the synthesized materials were compared with those of some perovskite NCs, as shown in Table S1. Figure 1a shows the crystal structure of  $\text{Cs}_2\text{CuCl}_4$ , where isolated tetrahedral  $\text{CuCl}_4^{2-}$  units were separated by the surrounding  $\text{Cs}^+$  ions. Figure 1b shows the XRD data of samples synthesized with different Cs:Cu precursor

ratios (0.6:1, 0.7:1 and 0.8:1). We found that a Cs: Cu ratio of 0.7:1 produced pure  $\text{Cs}_2\text{CuCl}_4$  (PDF#71-09-01). The diffraction peaks at  $20.6^\circ$ ,  $21.6^\circ$ ,  $22.8^\circ$ ,  $23.4^\circ$ ,  $24.5^\circ$ ,  $28.3^\circ$ ,  $28.9^\circ$ ,  $30.7^\circ$ ,  $33.3^\circ$ ,  $35.1^\circ$ ,  $37^\circ$ ,  $42.6^\circ$  and  $57^\circ$  corresponded to the (121), (201), (211), (130), (031), (230), (122), (311), (132), (330), (232), (332) and (541) crystal planes of orthorhombic  $\text{Cs}_2\text{CuCl}_4$ , respectively. When the ratio of the metal precursor was slightly changed to 0.6:1 and 0.8:1, additional peaks appeared in the XRD data at  $43.9^\circ$ ,  $49.4^\circ$  and  $54.5^\circ$ , corresponding to (200), (210) and (211) of CsCl (PDF# 05-0607). This was similar to previously reported CsCl impurities in  $\text{Cs}_3\text{Cu}_2\text{Cl}_5$  NCs [43]. Figure 1c shows a typical large-scale transmission electron microscopy (TEM) image indicating a uniform size distribution of the as-prepared colloidal  $\text{Cs}_2\text{CuCl}_4$  NCs. The  $\text{Cs}_2\text{CuCl}_4$  NCs had cubic structures with an average size of  $24 \pm 2.1$  nm.

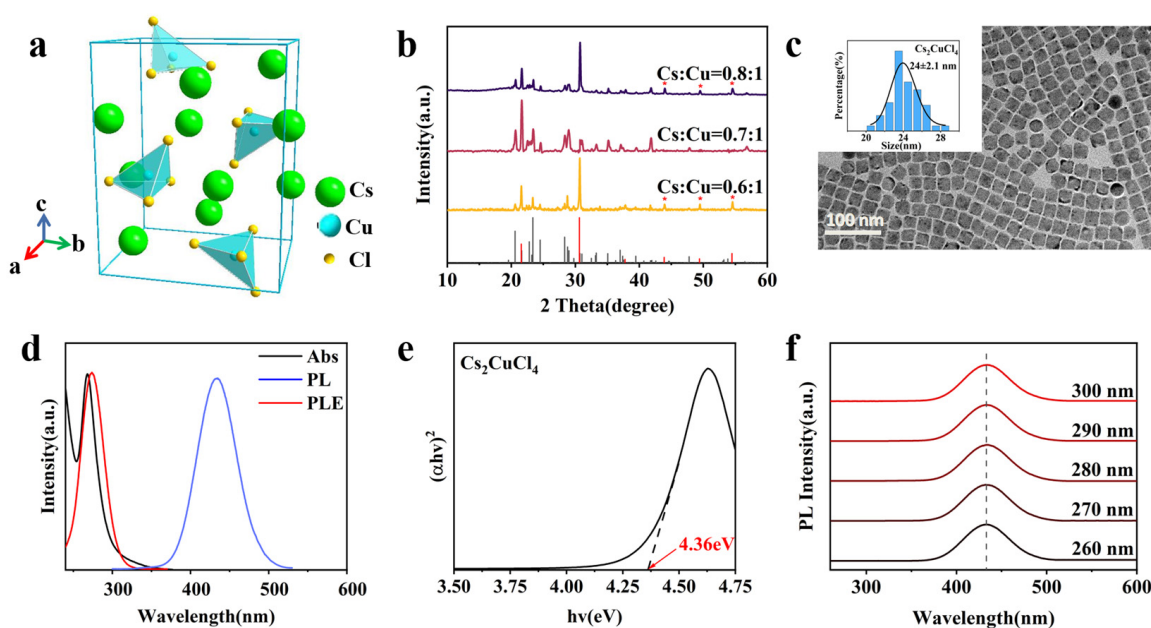


**Figure 1.** (a) Schematic crystal structure of  $\text{Cs}_2\text{CuCl}_4$  NCs; (b) XRD pattern of  $\text{Cs}_2\text{CuCl}_4$  NCs synthesized with different ratios of Cs:Cu (0.6:1, 0.7:1, 0.8:1) where the CsCl peaks are marked as red stars. The bottom plot is the standard XRD pattern of  $\text{Cs}_2\text{CuCl}_4$  (black lines, PDF#71-09-01) and CsCl (red lines, PDF#05-06-07); (c) TEM image of  $\text{Cs}_2\text{CuCl}_4$  NCs. The insets show the size distribution; (d) UV-Vis absorption, PLE, and PL spectra of  $\text{Cs}_2\text{CuCl}_4$  NCs. Inset: photographs of  $\text{Cs}_2\text{CuCl}_4$  NCs under ambient light (left) and 254 nm UV light excitation (right); (e) tauc plot of UV-Vis absorption of  $\text{Cs}_2\text{CuCl}_4$  NCs; (f) PL spectra of  $\text{Cs}_2\text{CuCl}_4$  NCs excited at different wavelengths (260 nm to 300 nm).

The UV-Vis absorption spectra of  $\text{Cs}_2\text{CuCl}_4$  NCs are presented in Figure 1d. The  $\text{Cs}_2\text{CuCl}_4$  NCs showed a strong excitonic absorption peak at around 268 nm. In addition, the band gap of the  $\text{Cs}_2\text{CuCl}_4$  NCs was measured by using the direct band gap tauc plot in Figure 1e, which shows a 4.36 eV band gap for  $\text{Cs}_2\text{CuCl}_4$  NCs. The PL spectrum (Figure 1d) of deep blue  $\text{Cs}_2\text{CuCl}_4$  NCs exhibited an emission peak at 434 nm (PLQY = 28.8%) with a full width at half-maximum (FWHM) of roughly 58 nm, which matched with  $\text{Cs}_2\text{CuCl}_4$  nanoplates [49]. The inset shows that  $\text{Cs}_2\text{CuCl}_4$  NCs had excellent luminescence performances of strong deep blue emissions under ultraviolet irradiation. The PL excitation (PLE) spectrum (monitoring emission at 434 nm) had a peak at 270 nm. The PLE spectrum matched with the exciton peak in the absorption spectrum, showing an apparent exciton characteristic of  $\text{Cs}_2\text{CuCl}_4$  NCs. The luminescence origin of NCs was studied by monitoring the PL spectra at different excitation wavelengths. Figure 1f shows that PL spectra excited at different wavelength had the same characteristics, indicating that the emission originated from the same excited state relaxation.

We employed X-ray photoelectron spectroscopy (XPS) to examine the valence state of Cu in the  $\text{Cs}_2\text{CuCl}_4$  NCs. Figure 2a displays the XPS survey spectrum in the entire binding energy region of the aggregated  $\text{Cs}_2\text{CuCl}_4$  NCs, confirming the presence of  $\text{Cs}^+$ ,  $\text{Cu}^{2+}$  and  $\text{Cl}^-$  elements at the surface. The satellite peak in the narrow scan of the Cu 2p spectrum in Figure 2c indicated the presence of  $\text{Cu}^{2+}$  ions on the surface of  $\text{Cs}_2\text{CuCl}_4$  NCs [51].

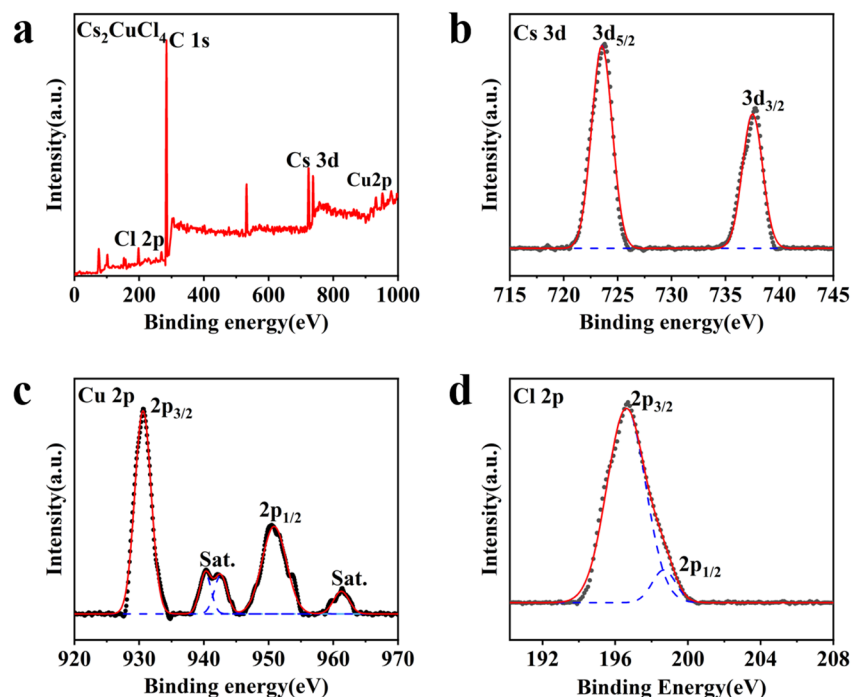


**Figure 2.** (a) XPS spectrum of  $\text{Cs}_2\text{CuCl}_4$  NCs; (b–d) The high-resolution XPS spectra, corresponding to Cs 3d, Cu 2p and Cl 2p, respectively. The black dashed lines represent experimental data, the blue dashed lines represent individual peak fitting and the red solid lines represent the sum of peak fitting.

The injection temperature is critical to the successful synthesis of  $\text{Cs}_2\text{CuCl}_4$  NCs. Although a high injection temperature can reduce the surface defects of NCs, it can also reduce the Cu(II) to Cu(I) through oleylamine and produce impurity phases [51]. Therefore, the highest PLQY was obtained by optimizing the experimental scheme to obtain an optimal injection temperature. The UV-Vis and PL spectra of different  $\text{Cs}_2\text{CuCl}_4$  NCs synthesized between 110 °C and 140 °C were compared in Figure 3a,b at the same concentration. The exciton absorption peak was highest for NCs synthesized between 120 °C and 130 °C, and the PL intensity was highest at 120 °C. These results indicate that the optimal injection temperature was 120 °C. We also examined the UV-Vis and PL spectra of  $\text{Cs}_2\text{CuCl}_4$  NCs synthesized with different Cs:Cu precursor ratios (Figure 3c,d). The highest exciton absorption peak and PL intensity were obtained from the sample synthesized with a Cs:Cu ratio of 0.7:1, indicating the best crystal quality of  $\text{Cs}_2\text{CuCl}_4$  NCs. This is consistent with the XRD result shown in Figure 1b, where other Cs:Cu ratios resulted in more CsCl impurities.

In addition, the ligands also play an important role in the synthesis of NCs. We found that the ratio between OA and OLA can affect the surface defects and stability of  $\text{Cs}_2\text{CuCl}_4$  NCs. Figure 3e shows the UV-Vis spectrum of the sample with different OA:OLA ligand ratios (0.5 mL:0.5 mL, 1.0 mL:0.5 mL; 0.5 mL:1.0 mL and 1.0 mL:1.0 mL). Both the exciton absorption peak and PL intensity were lowest when OA = 0.5 mL and OLA = 1 mL. Increasing the amount of OA and reducing OLA could significantly increase the absorption and PL intensity. This is due to excessive OLA being able to promote the reduction of Cu(II) to Cu(I) at a high temperature, while an adequate OA ligand can reduce the defect density on the  $\text{Cs}_2\text{CuCl}_4$  NCs surface. Therefore, in order to obtain  $\text{Cs}_2\text{CuCl}_4$  NCs with the highest crystal quality, the amount of ligand should be controlled to OA = 1.0 mL and OLA = 0.5 mL.

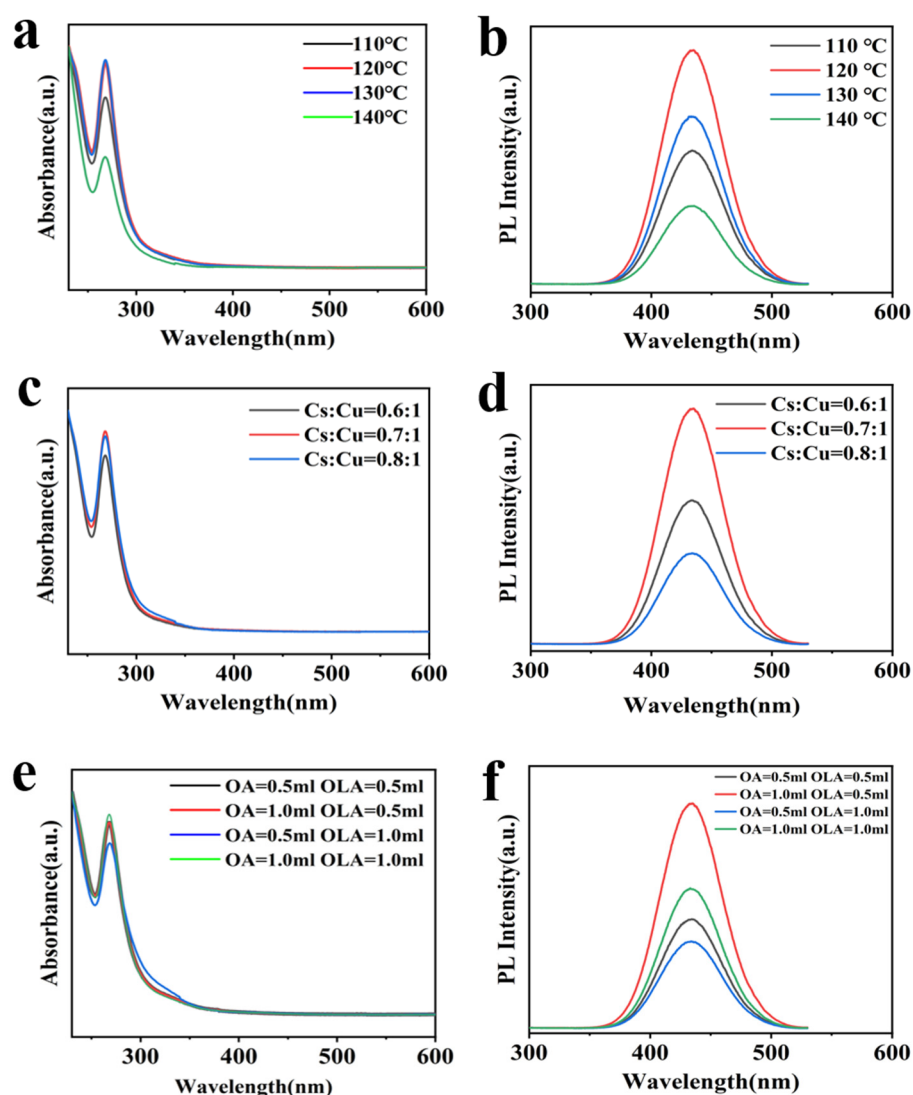


**Figure 3.** (a) UV-Vis absorption, (b) PL spectra of  $\text{Cs}_2\text{CuCl}_4$  NCs under different injection temperatures (110 °C, 120 °C, 130 °C, 140 °C); (c) UV-Vis absorption, (d) PL spectra of  $\text{Cs}_2\text{CuCl}_4$  NCs synthesized with different ratios of Cs:Cu (0.6:1, 0.7:1, 0.8:1); (e) UV-Vis absorption, (f) PL spectra of  $\text{Cs}_2\text{CuCl}_4$  NCs synthesized with different amounts of OA:OLA (1 mL:1 mL, 0.5 mL:1 mL, 1 mL:0.5 mL, 0.5 mL:0.5 mL).

The presence of OA and OLA ligands was further confirmed with Fourier transform infrared spectroscopy (FTIR) (Figure S1) [49]. The peak at  $1470\text{ cm}^{-1}$  represented the  $\text{COO}^-$  stretching vibration mode of OA. The peak at  $1720\text{ cm}^{-1}$  represented the asymmetrical vibration mode of OA. The peaks at  $2855\text{ cm}^{-1}$  and  $2905\text{ cm}^{-1}$  represented the vibration due to the stretching of the C-H bonds of  $-\text{CH}_3$  and  $-\text{CH}_2$  in the aliphatic hydrocarbon chain. The peak at  $1624\text{ cm}^{-1}$  represented the bending vibration of N-H scissors of the  $-\text{NH}_2$  group in OLA. The above results represent the stable existence of OA and OLA ligands on the  $\text{Cs}_2\text{CuCl}_4$  NCs surface.

We also investigated the effects of different halide precursors on the synthesis of  $\text{Cs}_2\text{CuCl}_4$  NCs. Bz-X and TMS-X ( $X = \text{Cl, Br, I}$ ) are commonly used halide precursors for lead halide perovskites. For example, Manna et al. [52] used Bz-X ( $X = \text{Cl, Br, I}$ ) to synthesize  $\text{APbX}_3$  NCs. TMS-X ( $X = \text{Cl, Br, I}$ ) were also reported for the synthesis of double perovskite NCs [53]. Therefore, we focused on Bz-Cl and TMS-Cl for the synthesis of  $\text{Cs}_2\text{CuCl}_4$  NCs. Due to the poor reactivity of TMS-Cl, the general reaction temperature was as high as  $180\text{ }^\circ\text{C}$ . In contrast, Bz-Cl had a higher reactivity and only needed  $120\text{ }^\circ\text{C}$  for the synthesis of NCs. Comparing the UV-Vis absorption and PL spectra of samples synthesized using

different Cl precursors (Figure S2), Bz-Cl had a higher absorption and PL intensity than TMS-Cl. Therefore, Bz-Cl was selected as the halide precursor to form pure phase  $\text{Cs}_2\text{CuCl}_4$  NCs with bright deep blue emissions. In addition to  $\text{Cs}_2\text{CuCl}_4$  NCs, we also tested the synthesis of  $\text{Cs}_2\text{CuBr}_4$  NCs. However, when using benzoyl bromine as the halide precursor, the presence of bromine will promote the reduction of Cu(II) to Cu(I), then form  $\text{Cs}_3\text{Cu}_2\text{Br}_5$  instead of  $\text{Cs}_2\text{CuBr}_4$ . The characterization of  $\text{Cs}_3\text{Cu}_2\text{Br}_5$  NCs are summarized in Figure S3. The  $\text{Cs}_3\text{Cu}_2\text{Br}_5$  NCs showed a strong excitonic absorption peak at around 270 nm and a PL emission peak at 454 nm. The XPS measurement of the Cu 2p spectrum in Figure S3e indicated the presence of Cu(I) ions in  $\text{Cs}_3\text{Cu}_2\text{Br}_5$  NCs [43].

The passivation of NCs with Ag to reduce surface defects is an effective method to improve the PLQY and stability of perovskite NCs [30,54]. For example, Li et al. [54] used the Ag-trioctylphosphine (Ag-TOP) complex to reduce surface defects and improve the PLQY and stability of  $\text{CsPbBr}_3$  NCs significantly. However, TOP cannot coexist with Cu(II) due to its strong reducibility at room temperature [55]. Therefore, we developed a simple and effective method for the passivation of  $\text{Cs}_2\text{CuCl}_4$  nanocrystals by combining oylamine with silver acetate to form an oylamine silver complex (Ag-OLA) as the passivation agent. We found that a small amount ( $\mu\text{L}$ ) of Ag-OLA solution could effectively bind chloride on the  $\text{Cs}_2\text{CuCl}_4$  NCs surface, reducing the surface traps caused by the loss of unstable ammonium chloride. Different amounts of Ag-OLA solution were added into a 3 mL  $\text{Cs}_2\text{CuCl}_4$  NCs colloidal solution, and the absorption (Figure 4a) and PL spectra (Figure 4b) were measured 2 min later. Compared with the untreated sample, the absorbance of Ag-treated  $\text{Cs}_2\text{CuCl}_4$  NCs increased slightly, but the peak position remained unchanged for different amounts of Ag-OLA solution. The PL intensity of  $\text{Cs}_2\text{CuCl}_4$  NCs first increased as the amount of Ag-OLA solution increased due to the surface passivation effect. The PLQY reached the highest value of 42% with 15  $\mu\text{L}$  Ag-OLA, which was nearly 70% higher than that of the untreated sample. Adding more Ag-OLA eventually led to a lower PLQY, owing to the formation of AgCl, which damaged the surface of  $\text{Cs}_2\text{CuCl}_4$  NCs. Note that the treatment was applied at room temperature, therefore the Ag ions were unlikely to dope inside  $\text{Cs}_2\text{CuCl}_4$  NCs. This is also supported by the unchanged PL peak position, demonstrating that no Cu-Ag alloyed NCs were formed [56].

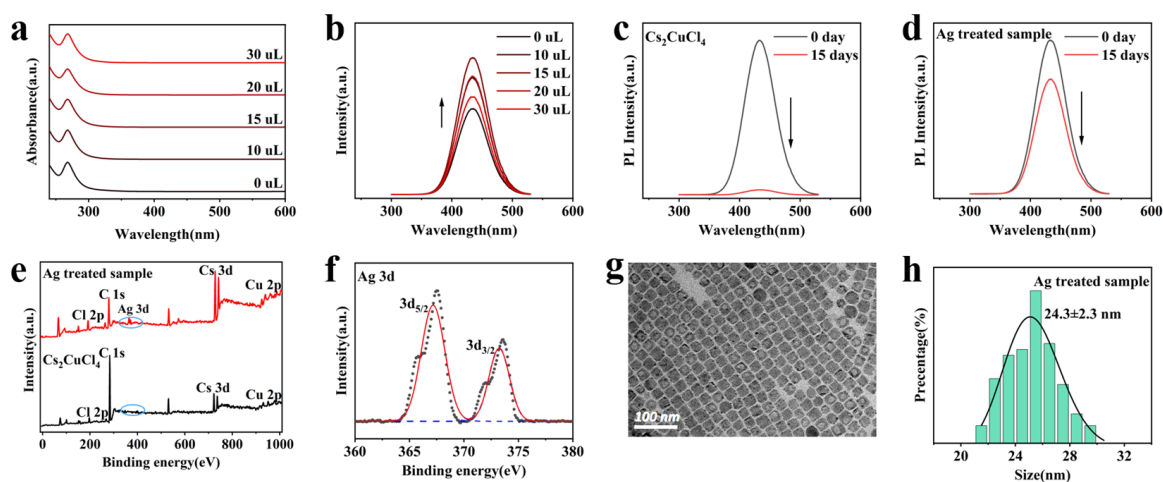


**Figure 4.** (a) Absorption spectra of  $\text{Cs}_2\text{CuCl}_4$  NCs and Ag-treated samples dispersed in hexane by adding different volumes of Ag-OLA reagent. (b) The evolution of PL spectra of Ag-treated  $\text{Cs}_2\text{CuCl}_4$  NCs. Highest PL was achieved by adding 15  $\mu\text{L}$  Ag-OLA. Changes in PL intensity of (c)  $\text{Cs}_2\text{CuCl}_4$  NCs and (d) Ag-treated sample after 15 days of storage, demonstrating the excellent stability of Ag-treated sample. (e) XPS spectrum of  $\text{Cs}_2\text{CuCl}_4$  NCs before and after Ag treatment. The Ag peaks can be clearly seen. (f) High-resolution Ag 3d spectrum of Ag-treated samples indicates the Ag(I) state. (g) TEM image of the Ag-treated  $\text{Cs}_2\text{CuCl}_4$  NCs. (h) Size distribution histogram of the Ag-treated  $\text{Cs}_2\text{CuCl}_4$  NCs.

In addition, we studied the air stability of Ag-treated Cs<sub>2</sub>CuCl<sub>4</sub> NCs in an ambient environment (average temperature 25 °C, humidity 50%). As shown in Figure 4d, Ag-treated Cs<sub>2</sub>CuCl<sub>4</sub> NCs maintained ~75% of their initial PLQY after a 15-day storage period, while the PLQY of untreated NCs decreased to 1% of their initial value, demonstrating the excellent air stability of the Ag-treated Cs<sub>2</sub>CuCl<sub>4</sub> NCs. Importantly, as shown in Figure S4, individual OLA could not increase the PL intensity of Cs<sub>2</sub>CuCl<sub>4</sub> NCs, proving that Ag plays a key role in enhancing the PLQY of Cs<sub>2</sub>CuCl<sub>4</sub> NCs. The existence of Ag on the surface of Cs<sub>2</sub>CuCl<sub>4</sub> NCs was verified by XPS, as shown in Figure 4e, where the Ag peaks can be clearly seen from the Ag-treated Cs<sub>2</sub>CuCl<sub>4</sub> NCs. Figure 4f indicates that Ag existed on the surface of Cs<sub>2</sub>CuCl<sub>4</sub> NCs in the form of Ag (I) in the oxidation state. The Ag-treated NCs present a regular cubic shape and size distributions at Figure 4g, with little change compared with the untreated ones.

The origin of the bright blue emission of Cs<sub>2</sub>CuCl<sub>4</sub> NCs can be attributed to the Cu ion induced traps. Manna et al. [57] found that doping Cu<sup>+</sup> into Cs<sub>2</sub>ZnCl<sub>4</sub> NCs can achieve a bright blue emission due to the Cu(I) ions promoting the formation of trapped excitons. In addition, Xu et al. [58] proposed that the emissions from Cu-doped ZnO nanorods originated from a Cu(II) defect. Therefore, we propose the schematic model of the luminescence mechanism of Cs<sub>2</sub>CuCl<sub>4</sub> NCs in Figure S5. Under UV light excitation, electrons transition from the ground state to the photoexcited state, and then undergo a non-radiative compound transition to the Cu<sup>2+</sup> defect state. The electrons at the defect level transition back to the ground state as a radiative recombination, exhibiting a broad spectrum of deep blue luminescence.

#### 4. Conclusions

We successfully synthesized pure phase Cs<sub>2</sub>CuCl<sub>4</sub> NCs with well-defined shapes via a modified hot-injection synthesis strategy. The effects of injection temperature, the Cu:Cs metal precursor ratio, the OA:OLA ligand ratio and the halide precursors were studied systematically. Through optimizing the synthesis conditions, the Cs<sub>2</sub>CuCl<sub>4</sub> NCs showed a high PLQY (28.8%) with deep blue emission at 434 nm. The PLQY and stability of Cs<sub>2</sub>CuCl<sub>4</sub> NCs can be further enhanced through Ag treatment using Ag-OLA complex, where Ag-treated Cs<sub>2</sub>CuCl<sub>4</sub> NCs exhibit higher PLQY (42%) and much improved stability in an ambient environment. This work provides an effective strategy for the synthesis of Cu(II)-based metal halide perovskite NCs, which are promising materials for reducing the toxicity and realizing practical applications of perovskite NCs for display and lighting devices.

**Supplementary Materials:** The following supporting information can be downloaded at: <https://www.mdpi.com/article/10.3390/cryst13060864/s1>. Table S1. Summary of the optical performance of the lead and lead-free perovskite NCs. Figure S1. The FTIR spectra of Cs<sub>2</sub>CuCl<sub>4</sub> NCs. Figure S2. (a) UV-Vis spectra from NCs synthesized using different precursors (Bz-Cl and TMS-Cl). (b) PL spectra for samples synthesized using different precursors (Bz-Cl and TMS-Cl). Figure S3. (a) TEM images of the Cs<sub>3</sub>Cu<sub>2</sub>Br<sub>5</sub> NCs. (b) UV-Vis absorption, PLE and PL spectra of Cs<sub>3</sub>Cu<sub>2</sub>Br<sub>5</sub> NCs. (c) XPS survey scan of Cs<sub>3</sub>Cu<sub>2</sub>Br<sub>5</sub> NCs. (d–f) The high-resolution XPS spectra corresponding to Cs 3d, Cu 2p and Br 3d, respectively. Figure S4. (a) PL spectra for Cs<sub>2</sub>CuCl<sub>4</sub> NCs and Ag-treated samples. (b) PL spectra for Cs<sub>2</sub>CuCl<sub>4</sub> NCs and Cs<sub>2</sub>CuCl<sub>4</sub>-OLA. Figure S5. Schematic model representing the emission mechanism.

**Author Contributions:** Conceptualization, H.L.; Methodology, W.G.; Data curation, Y.Z.; Writing—original draft preparation, W.G. and Y.Z.; Writing—review and editing, H.L., F.L. and J.W.; Resources, Y.D., P.H. and G.J. All authors have read and agreed to the published version of the manuscript.

**Funding:** This research was funded by the National Natural Science Foundation of China (22179009, 22005034).

**Data Availability Statement:** Not applicable.

**Conflicts of Interest:** The authors declare no conflict of interest.

## References

1. Ling, X.; Zhou, S.; Yuan, J.; Shi, J.; Qian, Y.; Larson, B.W.; Zhao, Q.; Qin, C.; Li, F.; Shi, G.; et al. 14.1% CsPbI<sub>3</sub> Perovskite Quantum Dot Solar Cells via Cesium Cation Passivation. *Adv. Energy Mater.* **2019**, *9*, 1900721. [[CrossRef](#)]
2. Li, C.-H.A.; Zhou, Z.; Vashishtha, P.; Halpert, J.E. The Future Is Blue (LEDs): Why Chemistry Is the Key to Perovskite Displays. *Chem. Mater.* **2019**, *31*, 6003–6032. [[CrossRef](#)]
3. Zhu, H.; Fu, Y.; Meng, F.; Wu, X.; Gong, Z.; Ding, Q.; Gustafsson, M.V.; Trinh, M.T.; Jin, S.; Zhu, X.-Y. Lead halide perovskite nanowire lasers with low lasing thresholds and high quality factors. *Nat. Mater.* **2015**, *14*, 636–642. [[CrossRef](#)] [[PubMed](#)]
4. Zhu, Y.; Liu, Y.; Mill, K.A.; Zhu, H.; Egap, E. Lead Halide Perovskite Nanocrystals as Photocatalysts for PET-RAFT Polymerization under Visible and Near-Infrared Irradiation. *ACS Macro Lett.* **2020**, *9*, 725–730. [[CrossRef](#)] [[PubMed](#)]
5. Jin, X.; Ma, K.; Gao, H. Tunable Luminescence and Enhanced Polar Solvent Resistance of Perovskite Nanocrystals Achieved by Surface-Initiated Photopolymerization. *J. Am. Chem. Soc.* **2022**, *144*, 20411–20420. [[CrossRef](#)]
6. Wang, F.; Zou, X.; Xu, M.; Wang, H.; Wang, H.; Guo, H.; Guo, J.; Wang, P.; Peng, M.; Wang, Z.; et al. Recent Progress on Electrical and Optical Manipulations of Perovskite Photodetectors. *Adv. Sci.* **2021**, *8*, e2100569. [[CrossRef](#)]
7. Shamsi, J.; Urban, A.S.; Imran, M.; De Trizio, L.; Manna, L. Metal Halide Perovskite Nanocrystals: Synthesis, Post-Synthesis Modifications, and Their Optical Properties. *Chem. Rev.* **2019**, *119*, 3296–3348. [[CrossRef](#)]
8. Ng, C.K.; Wang, C.; Jasieniak, J.J. Synthetic Evolution of Colloidal Metal Halide Perovskite Nanocrystals. *Langmuir* **2019**, *35*, 11609–11628. [[CrossRef](#)]
9. Akkerman, Q.A.; D'innocenzo, V.; Accornero, S.; Scarpellini, A.; Petrozza, A.; Prato, M.; Manna, L. Tuning the Optical Properties of Cesium Lead Halide Perovskite Nanocrystals by Anion Exchange Reactions. *J. Am. Chem. Soc.* **2015**, *137*, 10276–10281. [[CrossRef](#)]
10. Protesescu, L.; Yakunin, S.; Bodnarchuk, M.I.; Krieg, F.; Caputo, R.; Hendon, C.H.; Yang, R.X.; Walsh, A.; Kovalenko, M.V. Nanocrystals of Cesium Lead Halide Perovskites (CsPbX<sub>3</sub>, X = Cl, Br, and I): Novel Optoelectronic Materials Showing Bright Emission with Wide Color Gamut. *Nano Lett.* **2015**, *15*, 3692–3696. [[CrossRef](#)]
11. Song, J.; Li, J.; Li, X.; Xu, L.; Dong, Y.; Zeng, H. Quantum Dot Light-Emitting Diodes Based on Inorganic Perovskite Cesium Lead Halides (CsPbX<sub>3</sub>). *Adv. Mater.* **2015**, *27*, 7162–7167. [[CrossRef](#)] [[PubMed](#)]
12. Zheng, X.; Yuan, S.; Liu, J.; Yin, J.; Yuan, F.; Shen, W.-S.; Yao, K.; Wei, M.; Zhou, C.; Song, K.; et al. Chlorine Vacancy Passivation in Mixed Halide Perovskite Quantum Dots by Organic Pseudohalides Enables Efficient Rec. 2020 Blue Light-Emitting Diodes. *ACS Energy Lett.* **2022**, *5*, 793–798. [[CrossRef](#)]
13. Pan, G.; Bai, X.; Xu, W.; Chen, X.; Zhai, Y.; Zhu, J.; Shao, H.; Ding, N.; Xu, L.; Dong, B.; et al. Bright Blue Light Emission of Ni<sup>2+</sup> Ion-Doped CsPbCl<sub>x</sub>Br<sub>3-x</sub> Perovskite Quantum Dots Enabling Efficient Light-Emitting Devices. *ACS Appl. Mater. Interfaces* **2020**, *12*, 14195–14202. [[CrossRef](#)] [[PubMed](#)]
14. Ji, K.; Anaya, M.; Abfalterer, A.; Stranks, S.D. Halide Perovskite Light-Emitting Diode Technologies. *Adv. Opt. Mater.* **2021**, *9*, 2002128. [[CrossRef](#)]
15. Luo, M.; Jiang, Y.; He, T.; Yuan, M. Metal halide perovskites for blue light emitting materials. *APL Mater.* **2020**, *8*, 040907. [[CrossRef](#)]
16. Kim, Y.H.; Kim, S.; Kakekhani, A.; Park, J.; Park, J.; Lee, Y.H.; Xu, H.; Nagane, S.; Wexler, R.B.; Kim, D.H.; et al. Comprehensive defect suppression in perovskite nanocrystals for high-efficiency light-emitting diodes. *Nat. Photonics* **2021**, *15*, 148–155. [[CrossRef](#)]
17. Zhu, L.; Cao, H.; Xue, C.; Zhang, H.; Qin, M.; Wang, J.; Wen, K.; Fu, Z.; Jiang, T.; Xu, L.; et al. Unveiling the additive-assisted oriented growth of perovskite crystallite for high performance light-emitting diodes. *Nat. Commun.* **2021**, *12*, 5081. [[CrossRef](#)]
18. Zhou, Y.-H.; Wang, C.; Yuan, S.; Zou, C.; Su, Z.; Wang, K.-L.; Xia, Y.; Wang, B.; Di, D.; Wang, Z.-K.; et al. Stabilized Low-Dimensional Species for Deep-Blue Perovskite Light-Emitting Diodes with EQE Approaching 3.4%. *J. Am. Chem. Soc.* **2022**, *144*, 18470–18478. [[CrossRef](#)]
19. Zhang, C.; Wan, Q.; Ono, L.K.; Liu, Y.; Zheng, W.; Zhang, Q.; Liu, M.; Kong, L.; Li, L.; Qi, Y. Narrow-Band Violet-Light-Emitting Diodes Based on Stable Cesium Lead Chloride Perovskite Nanocrystals. *ACS Energy Lett.* **2021**, *6*, 3545–3554. [[CrossRef](#)]
20. Jiang, J.; Chu, Z.; Yin, Z.; Li, J.; Yang, Y.; Chen, J.; Wu, J.; You, J.; Zhang, X. Red Perovskite Light-Emitting Diodes with Efficiency Exceeding 25% Realized by Co-Spacer Cations. *Adv. Mater.* **2022**, *34*, 2204460. [[CrossRef](#)]
21. Li, X.; Wu, Y.; Zhang, S.; Cai, B.; Gu, Y.; Song, J.; Zeng, H. CsPbX<sub>3</sub> Quantum Dots for Lighting and Displays: Room-Temperature Synthesis, Photoluminescence Superiorities, Underlying Origins and White Light-Emitting Diodes. *Adv. Funct. Mater.* **2016**, *26*, 2435–2445. [[CrossRef](#)]
22. Dong, Y.; Wang, Y.-K.; Yuan, F.; Johnston, A.; Liu, Y.; Ma, D.; Choi, M.-J.; Chen, B.; Chekini, M.; Baek, S.-W.; et al. Bipolar-shell resurfacing for blue LEDs based on strongly confined perovskite quantum dots. *Nat. Nanotechnol.* **2020**, *15*, 668–674. [[CrossRef](#)] [[PubMed](#)]
23. Lu, C.-H.; Biesold-McGee, G.V.; Liu, Y.; Kang, Z.; Lin, Z. Doping and ion substitution in colloidal metal halide perovskite nanocrystals. *Chem. Soc. Rev.* **2020**, *49*, 4953–5007. [[CrossRef](#)]
24. Jellicoe, T.C.; Richter, J.M.; Glass, H.F.J.; Tabachnyk, M.; Brady, R.; Dutton, S.E.; Rao, A.; Friend, R.H.; Credgington, D.; Greenham, N.C.; et al. Synthesis and Optical Properties of Lead-Free Cesium Tin Halide Perovskite Nanocrystals. *J. Am. Chem. Soc.* **2016**, *138*, 2941–2944. [[CrossRef](#)] [[PubMed](#)]
25. Wu, X.; Song, W.; Li, Q.; Zhao, X.; He, D.; Quan, Z. Synthesis of Lead-free CsGeI<sub>3</sub> Perovskite Colloidal Nanocrystals and Electron Beam-induced Transformations. *Chem. Asian J.* **2018**, *13*, 1654–1659. [[CrossRef](#)] [[PubMed](#)]

26. Swarnkar, A.; Ravi, V.K.; Nag, A. Beyond Colloidal Cesium Lead Halide Perovskite Nanocrystals: Analogous Metal Halides and Doping. *ACS Energy Lett.* **2017**, *2*, 1089–1098. [[CrossRef](#)]
27. Kang, C.; Rao, H.; Fang, Y.; Zeng, J.; Pan, Z.; Zhong, X. Antioxidative Stannous Oxalate Derived Lead-Free Stable CsSnX<sub>3</sub> (X = Cl, Br, and I) Perovskite Nanocrystals. *Angew. Chem. Int. Ed.* **2021**, *60*, 660–665. [[CrossRef](#)] [[PubMed](#)]
28. Wei, Y.; Li, K.; Cheng, Z.; Liu, M.; Xiao, H.; Dang, P.; Liang, S.; Wu, Z.; Lian, H.; Lin, J. Epitaxial Growth of CsPbX<sub>3</sub> (X = Cl, Br, I) Perovskite Quantum Dots via Surface Chemical Conversion of Cs<sub>2</sub>GeF<sub>6</sub> Double Perovskites: A Novel Strategy for the Formation of Leadless Hybrid Perovskite Phosphors with Enhanced Stability. *Adv. Mater.* **2019**, *31*, 1807592. [[CrossRef](#)] [[PubMed](#)]
29. Lou, Y.; Fang, M.; Chen, J.; Zhao, Y. Formation of highly luminescent cesium bismuth halide perovskite quantum dots tuned by anion exchange. *Chem. Commun.* **2018**, *54*, 3779–3782. [[CrossRef](#)] [[PubMed](#)]
30. Li, T.; Ma, J.; Qiao, M.; Kuang, Y.; He, Y.; Ran, X.; Guo, L.; Wang, X. Enhanced blue photoluminescence and photostability of Cs<sub>3</sub>Bi<sub>2</sub>Br<sub>9</sub> perovskite quantum dots via surface passivation with silver ions. *Crystengcomm* **2021**, *23*, 7219–7227. [[CrossRef](#)]
31. Ma, Z.; Shi, Z.; Yang, D.; Zhang, F.; Li, S.; Wang, L.; Wu, D.; Zhang, Y.; Na, G.; Zhang, L.; et al. Electrically-Driven Violet Light-Emitting Devices Based on Highly Stable Lead-Free Perovskite Cs<sub>3</sub>Sb<sub>2</sub>Br<sub>9</sub> Quantum Dots. *ACS Energy Lett.* **2020**, *5*, 385–394. [[CrossRef](#)]
32. Locardi, F.; Cirignano, M.; Baranov, D.; Dang, Z.; Prato, M.; Drago, F.; Ferretti, M.; Pinchetti, V.; Fanciulli, M.; Brovelli, S.; et al. Colloidal Synthesis of Double Perovskite Cs<sub>2</sub>AgInCl<sub>6</sub> and Mn-Doped Cs<sub>2</sub>AgInCl<sub>6</sub> Nanocrystals. *J. Am. Chem. Soc.* **2018**, *140*, 12989–12995. [[CrossRef](#)] [[PubMed](#)]
33. Kung, P.; Li, M.; Lin, P.; Jhang, J.; Pantaler, M.; Lupascu, D.C.; Grancini, G.; Chen, P. Lead-Free Double Perovskites for Perovskite Solar Cells. *Sol. RRL* **2020**, *4*, 1900306. [[CrossRef](#)]
34. Bekenstein, Y.; Dahl, J.C.; Huang, J.; Osowiecki, W.T.; Swabeck, J.K.; Chan, E.M.; Yang, P.; Alivisatos, A.P. The Making and Breaking of Lead-Free Double Perovskite Nanocrystals of Cesium Silver–Bismuth Halide Compositions. *Nano Lett.* **2018**, *18*, 3502–3508. [[CrossRef](#)] [[PubMed](#)]
35. Volonakis, G.; Filip, M.R.; Haghighirad, A.A.; Sakai, N.; Wenger, B.; Snaith, H.J.; Giustino, F. Lead-Free Halide Double Perovskites via Heterovalent Substitution of Noble Metals. *J. Phys. Chem. Lett.* **2016**, *7*, 1254–1259. [[CrossRef](#)]
36. Cai, T.; Shi, W.; Hwang, S.; Kobbekaduwa, K.; Nagaoka, Y.; Yang, H.; Kimball, K.; Zhu, H.; Wang, J.; Wang, Z.; et al. Lead-Free Cs<sub>4</sub>CuSb<sub>2</sub>Cl<sub>12</sub> Layered Double Perovskite Nanocrystals. *J. Am. Chem. Soc.* **2020**, *142*, 11927–11936. [[CrossRef](#)]
37. Liu, M.; Matta, S.; Ali-Löyty, H.; Matuhina, A.; Grandhi, G.K.; Lahtonen, K.; Russo, S.; Vivo, P. Moisture-Assisted near-UV Emission Enhancement of Lead-Free Cs<sub>4</sub>CuIn<sub>2</sub>Cl<sub>12</sub> Double Perovskite Nanocrystals. *Nano Lett.* **2022**, *22*, 311–318. [[CrossRef](#)] [[PubMed](#)]
38. Singhal, N.; Chakraborty, R.; Ghosh, P.; Nag, A. Low-Bandgap Cs<sub>4</sub>CuSb<sub>2</sub>Cl<sub>12</sub> Layered Double Perovskite: Synthesis, Reversible Thermal Changes, and Magnetic Interaction. *Chem. Asian J.* **2018**, *13*, 2085–2092. [[CrossRef](#)]
39. Vargas, B.; Torres-Cadena, R.; Reyes-Castillo, D.T.; Rodríguez-Hernández, J.; Gembicky, M.; Menéndez-Proupin, E.; Solis-Ibarra, D. Chemical Diversity in Lead-Free, Layered Double Perovskites: A Combined Experimental and Computational Approach. *Chem. Mater.* **2020**, *32*, 424–429. [[CrossRef](#)]
40. Li, Y.; Zhou, Z.; Tewari, N.; Ng, M.; Geng, P.; Chen, D.; Ko, P.K.; Qammar, M.; Guo, L.; Halpert, J.E. Progress in copper metal halides for optoelectronic applications. *Mater. Chem. Front.* **2021**, *5*, 4796–4820. [[CrossRef](#)]
41. Cheng, P.; Sun, L.; Feng, L.; Yang, S.; Yang, Y.; Zheng, D.; Zhao, Y.; Sang, Y.; Zhang, R.; Wei, D.; et al. Colloidal Synthesis and Optical Properties of All-Inorganic Low-Dimensional Cesium Copper Halide Nanocrystals. *Angew. Chem. Int. Ed.* **2019**, *58*, 16087–16091. [[CrossRef](#)] [[PubMed](#)]
42. Wang, L.; Shi, Z.; Ma, Z.; Yang, D.; Zhang, F.; Ji, X.; Wang, M.; Chen, X.; Na, G.; Chen, S.; et al. Colloidal Synthesis of Ternary Copper Halide Nanocrystals for High-Efficiency Deep-Blue Light-Emitting Diodes with a Half-Lifetime above 100 h. *Nano Lett.* **2020**, *20*, 3568–3576. [[CrossRef](#)] [[PubMed](#)]
43. Li, Y.; Vashishtha, P.; Zhou, Z.; Li, Z.; Shivarudraiah, S.B.; Ma, C.; Liu, J.; Wong, K.S.; Su, H.; Halpert, J.E. Room Temperature Synthesis of Stable, Printable Cs<sub>3</sub>Cu<sub>2</sub>X<sub>5</sub> (X = I, Br/I, Br, Br/Cl, Cl) Colloidal Nanocrystals with Near-Unity Quantum Yield Green Emitters (X = Cl). *Chem. Mater.* **2020**, *32*, 5515–5524. [[CrossRef](#)]
44. Lu, Y.; Li, G.; Fu, S.; Fang, S.; Li, L. CsCu<sub>2</sub>I<sub>3</sub> Nanocrystals: Growth and Structural Evolution for Tunable Light Emission. *ACS Omega* **2021**, *6*, 544–552. [[CrossRef](#)] [[PubMed](#)]
45. Vashishtha, P.; Hooper, T.J.N.; Fang, Y.; Kathleen, D.; Giovanni, D.; Klein, M.; Sum, T.; Mhaisalkar, S.; Mathews, N.; White, T. Room temperature synthesis of low-dimensional rubidium copper halide colloidal nanocrystals with near unity photoluminescence quantum yield. *Nanoscale* **2021**, *13*, 59–65. [[CrossRef](#)]
46. Zhou, Z.; Li, Y.; Xing, Z.; Li, Z.; Wong, K.S.; Halpert, J.E. Potassium and Rubidium Copper Halide A<sub>2</sub>CuX<sub>3</sub> (A = K, Rb, X = Cl, Br) Micro- and Nanocrystals with Near Unity Quantum Yields for White Light Applications. *ACS Appl. Nano Mater.* **2021**, *4*, 14188–14196. [[CrossRef](#)]
47. Chen, H.; Gao, Z.; Lv, P.; Sun, L.; Xu, C. Blue luminescence of Cs<sub>2</sub>CuCl<sub>4</sub> glass ceramics with long-term water-resistance stability. *J. Non-Cryst. Solids* **2022**, *597*, 121867. [[CrossRef](#)]
48. Yang, P.; Liu, G.; Liu, B.; Liu, X.; Lou, Y.; Chen, J.; Zhao, Y. All-inorganic Cs<sub>2</sub>CuX<sub>4</sub> (X = Cl, Br, and Br/I) perovskite quantum dots with blue-green luminescence. *Chem. Commun.* **2018**, *54*, 11638–11641. [[CrossRef](#)]
49. Shankar, H.; Jha, A.; Kar, P. Water-assisted synthesis of lead-free Cu based fluorescent halide perovskite nanostructures. *Mater. Adv.* **2022**, *3*, 658–664. [[CrossRef](#)]

50. Booker, E.P.; Griffiths, G.T.; Eyre, L.; Ducati, C.; Greenham, N.C.; Davis, N.J.L.K. Synthesis, Characterization, and Morphological Control of Cs<sub>2</sub>CuCl<sub>4</sub> Nanocrystals. *J. Phys. Chem. C* **2019**, *123*, 16951–16956. [[CrossRef](#)]
51. Cortecchia, D.; Dewi, H.A.; Yin, J.; Bruno, A.; Chen, S.; Baikie, T.; Boix, P.P.; Gratzel, M.; Mhaisalkar, S.; Soci, C.; et al. Lead-Free MA<sub>2</sub>CuCl<sub>x</sub>Br<sub>4-x</sub> Hybrid Perovskites. *Inorg. Chem.* **2016**, *55*, 1044–1052. [[CrossRef](#)] [[PubMed](#)]
52. Imran, M.; Caligiuri, V.; Wang, M.; Goldoni, L.; Prato, M.; Krahne, R.; De Trizio, L.; Manna, L. Benzoyl Halides as Alternative Precursors for the Colloidal Synthesis of Lead-Based Halide Perovskite Nanocrystals. *J. Am. Chem. Soc.* **2018**, *140*, 2656–2664. [[CrossRef](#)] [[PubMed](#)]
53. Creutz, S.E.; Crites, E.N.; Siena, M.; Gamelin, D.R. Anion Exchange in Cesium Lead Halide Perovskite Nanocrystals and Thin Films Using Trimethylsilyl Halide Reagents. *Chem. Mater.* **2018**, *30*, 4887–4891.
54. Li, H.; Qian, Y.; Xing, X.; Zhu, J.; Huang, X.; Jing, Q.; Zhang, W.; Zhang, C.; Lu, Z. Enhancing Luminescence and Photostability of CsPbBr<sub>3</sub> Nanocrystals via Surface Passivation with Silver Complex. *J. Phys. Chem. C* **2018**, *122*, 12994–13000. [[CrossRef](#)]
55. Okada, S.; Nakahara, Y.; Watanabe, M.; Tamai, T.; Kobayashi, Y.; Yajima, S. Room-Temperature Coalescence of Tri-n-Octylphosphine-Oxide-Capped Cu-Ag Core-Shell Nanoparticles: Effect of Sintering Agent and/or Reducing Agent. *Bull. Chem. Soc. Jpn.* **2021**, *94*, 1616–1624. [[CrossRef](#)]
56. Ji, S.; Meng, X.; Wang, X.; Bai, T.; Zhang, R.; Yang, B.; Han, K.; Jiang, J.; Liu, F. Colloidal synthesis of size-confined CsAgCl<sub>2</sub> nanocrystals: Implications for electroluminescence applications. *Mater. Chem. Front.* **2022**, *6*, 3669–3677. [[CrossRef](#)]
57. Zhu, D.; Zaffalon, M.L.; Pinchetti, V.; Brescia, R.; Moro, F.; Fasoli, M.; Fanciulli, M.; Tang, A.; Infante, I.; Trizio, L.D.; et al. Bright Blue Emitting Cu-Doped Cs<sub>2</sub>ZnCl<sub>4</sub> Colloidal Nanocrystals. *Chem. Mater.* **2020**, *32*, 5897–5903. [[CrossRef](#)]
58. Xu, C.X.; Sun, X.; Zhang, X.H.; Ke, L.; Chua, S.J. Photoluminescent properties of copper-doped zinc oxide nanowires. *Nanotechnology* **2004**, *15*, 856–861. [[CrossRef](#)]

**Disclaimer/Publisher's Note:** The statements, opinions and data contained in all publications are solely those of the individual author(s) and contributor(s) and not of MDPI and/or the editor(s). MDPI and/or the editor(s) disclaim responsibility for any injury to people or property resulting from any ideas, methods, instructions or products referred to in the content.